Integrated Sensing in Robotic Skin Modules

William R. Johnson III, Joran Booth, and Rebecca Kramer-Bottiglio
Mechanical Engineering & Materials Science
Yale University
New Haven, Connecticut, USA
will.johnson@yale.edu, joran.booth@yale.edu, rebecca.kramer@yale.edu

2021 IEEE Sensors | 978-1-7281-9501-8/21/$31.00 ©2021 IEEE | DOI: 10.1109/SENSORS47087.2021.9639529

***Abstract*—Robotic skins combine actuation and sensing in a 2D, modular soft robot. Robotic skins can be attached to or wrapped around arbitrary objects to add robotic functionality, and they have been demonstrated in a variety of applications, including continuum robots and active wearables. However, the sensors and actuators in current robotic skins are not well integrated. The attachable and detachable components on robotic skins limit their efficiency and robustness compared to the biological systems with embedded multi-functionality they aim to rival. This work integrates sensors into active skins to create robotic skins with embedded actuation and sensing. Experiments demonstrate the skin's ability to reconstruct its perimeter within 0.59% and its vertex locations within 12.6% of its length scale. This work is the first step toward robotic skins with fully integrated sensing and actuation.**

***Index Terms*—shape reconstruction, robotic skins**

I. Introduction

Robotic skins are 2D soft robots that contain both actuation and sensing [1]. Robotic skins are modular and reconfigurable, and they can transform passive structures into soft robots when they are attached at the surface [2] or wrapped around a soft body [3]. Robotic skins have been demonstrated achieving shape change by sculpting clay [4] and learning their own models for closed-loop control [5]. There is a large body of literature on electronic, sensory skins inspired by biological skin [6]. Sensory skins can be adhered to the surface of soft bodies [7] [8] or placed at the surface of a soft robot during the fabrication process [9]. Sensory skins have been demonstrated with haptic sensing [8], texture sensing [10], and strain and pressure sensing [11] [12] suitable for a variety of soft robotic and wearable applications. In contrast, robotic skins, which integrate actuation and sensing, are relatively new with many opportunities for advancing the technology.

Current robotic skins are made from modular components that are not well integrated, resulting in failure at the attachment points between sensors, actuators, and substrates. Moreover, tighter integration of sensors and actuators leads to increased efficiency and previously unachievable functionality [13]. We have previously shown membrane actuators that have integrated actuation in active skins in the form of pneumatic bladders [14], which enabled larger deformations and increased robustness on a skin-based tensegrity robot. Proprioception is essential for effective control of soft robots [15]. Integrated sensing for proprioception can lead to improved robustness and more reliable control. This work integrates strain sensing into active skins toward tightly integrated robotic skins. We introduce a method for embedding sensors into well-integrated active skins and describe the one-time calibration process for the sensors. Experiments demonstrate the skin modules' reliable proprioception for soft robotic applications.

This material is based upon work supported by the National Science Foundation under grant no. IIS-1955225.

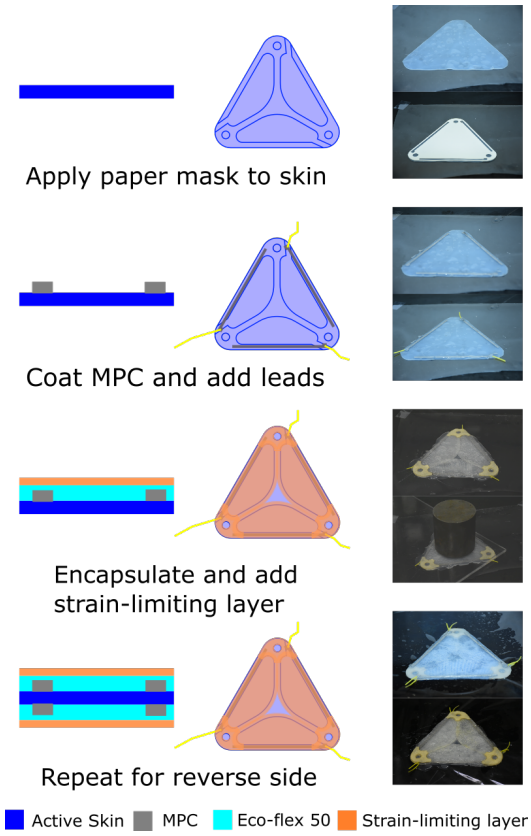

Fig. 1. Fabrication process for tightly integrated robotic skins. First, a multiphase composite (MPC) layer is coated on the active skin using a paper mask. After curing, the MPC layer is encapsulated, and the encapsulant doubles as glue to adhere the strain-limiting layer. These steps are repeated for the reverse side of the skin so that the two MPC layers together form capacitive sensors.

II. Module Fabrication

We chose to integrate capacitive strain sensors into the active skins due to their high accuracy, high linearity, cyclic stability, and negligible hysteresis [16]. In general, the capacitance of a parallel plate capacitor depends only on its

geometry, and a capacitive sensor behaves like a parallel plate capacitor if the electrode resistance is low [17]. In this work, we use a multiphase composite (MPC) that we developed in our previous work that has a notably low elecrical resistivity (4×10^{-5} Ω m) [18]. MPC is made from a silicone elastomer (Eco-Flex 50; Smooth-On), a room-temperature liquid metal (eutectic Gallium-Indium), and exfoliated intercalated graphite. In addition to its low resistivity, MPC is capable of high strains (200%) and can bond well to silicone substrates, making it a suitable choice for a soft sensor [18].

Following the manufacturing process shown in Fig. 1, the MPC sensors are embedded into an active skin made from a silicone elastomer (DragonSkin 10; Smooth-On) that has three inflatable pneumatic bladders. First, 100 mm x 3 mm strips of MPC are coated on top of the silicone skin using a 100 μm paper mask. Wire leads are inserted into the pre-cured composite on a 5 mm x 5 mm pad at the end of the strip, and the MPC is allowed to cure for two hours at room temperature. Next, a thin, encapsulating layer of Eco-Flex 50 is applied and used to adhere a strain-limiting layer. The strain-limiting layer consists of fabric reinforcements at the corners of the skin and a silicone composite with unidirectional inextensible fibers that limit strain anisotropically. For the manufacturing procedure of the strain-limiting layer (as well as the active skin without sensors), the reader is referred to [14]. The unidirectional fibers ensure that the capacitive sensors only experience strain transverse to the fibers' alignment and therefore only measure the strain in that direction. The skin is placed under a weight and the encapsulant/adhesive is allowed to cure for three hours at room temperature. Then, the skin is flipped over and the MPC and strain-limiting layers are coated on the reverse side in the same manner.

III. Experimental Methods

A. Sensor Calibration

Sensors were calibrated once before use. Each sensor was stretched to seven different known lengths between 120 mm (rest length) and 192 mm (60% strain), and the resulting capacitance was measured using a commercial capacitive sensing breakout board (MPR121; Adafruit). This calibration procedure was repeated three times for a total of 21 data points per sensor. The data were used to construct a linear model mapping capacitance to length for each sensor (Fig. 2a). All sensors exhibited high linearity with $R^2 > 0.99$. The standard deviation of the error between the linear model's prediction and the sensor's state in units of strain is 1.38% (Fig. 2b).

B. 2D Shape Reconstruction

To validate the shape reconstruction capabilities of the skin, experiments were done with a pegboard with 12 mm spacing between the holes (Fig. 3a) following the experimental procedure of [7]. A script output random coordinates on the pegboard within the sensors' calibrated range (120 mm to 192 mm), and the capacitance of each sensor was measured and converted into a length using the linear model corresponding to that sensor. The three lengths were used to reconstruct

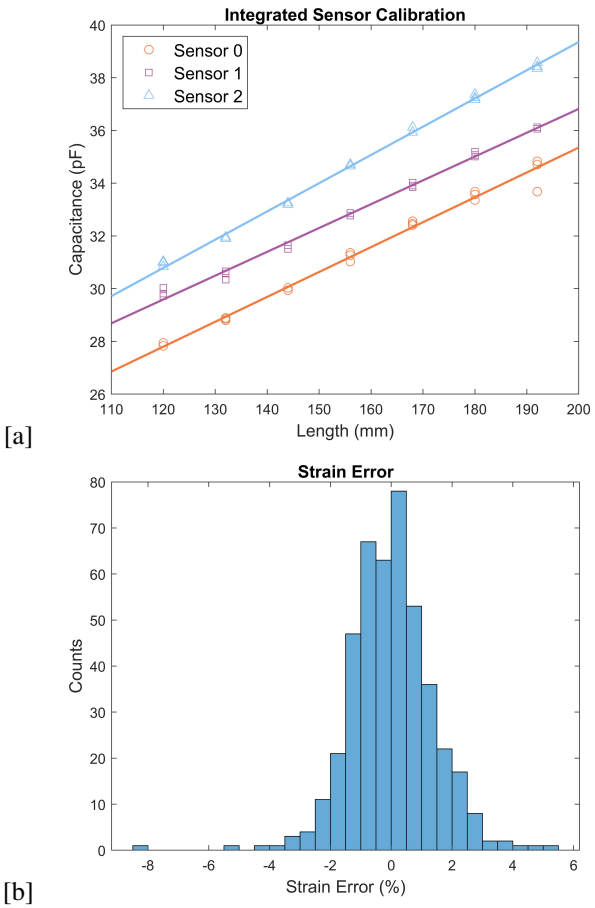

Fig. 2. Sensor calibration results. [a] Calibration data from three sensors on one skin. The markers represent the calibration trials, and the lines represent the linear fits. [b] Histogram of residuals from all sensor calibration trials in units of strain. $\sigma = 0.0138$.

the coordinates of the vertices of the triangle (Fig. 3b) using the same method as our previous work [7]:

$$x_0 = L_0 \tag{1}$$

$$x_1 = \frac{L_2^2 - L_1^2 + x_1^2}{2x_1} \tag{2}$$

$$y_2 = \sqrt{L_2^2 - x_2^2} \tag{3}$$

These variables are defined in Fig. 3a. One example from the reconstruction experiments is shown in Fig. 3b. Each of the seven skins was used for 20 reconstruction trials.

IV. Results

The shape reconstruction results are summarized in Fig. 4. We define the Euclidean error as the sum of the planar distances between the reconstructed vertices and the true vertex locations. While there are different ways to quantify the reconstruction error, we chose to show the Euclidean error, which is preferred in applications where the location of one vertex is known. If shape accuracy is more important, the

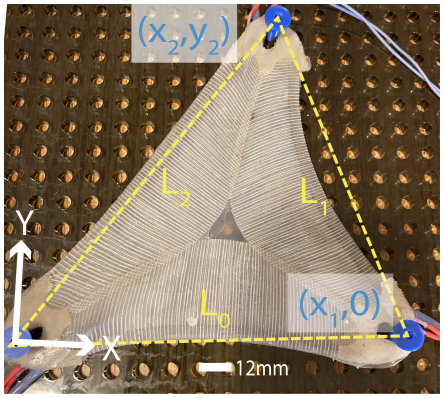

[a]

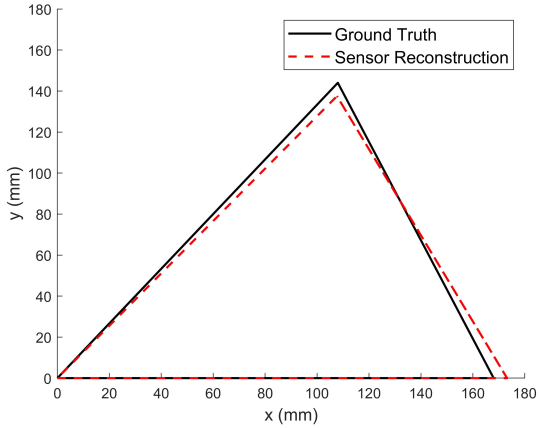

[b]

Fig. 3. (a) Experiments were conducted with the skins on an acrylic pegboard with 12 mm spacing between the holes. (b) An example of reconstruction. The black lines connect the points where the skin's vertices were placed on the pegboard, and the red lines represent the sensor reconstruction.

Procrustes error should be calculated as in [2]. The graph in Fig. 4a shows the average Euclidean error for each skin across 20 trials as an absolute distance on the right and normalized by the rest length (120 mm) of one side of the triangular skin on the left. The normalized Euclidean error from each of the 140 trials is plotted in Fig. 4b. The average normalized Euclidean error was 12.6% (15.1 mm on an absolute scale) with a standard deviation of 5.80% (6.96 mm). We also quantify the error in reconstructing the perimeter of the triangle. In the perimetric case (Fig. 4c), the average error over all skins and trials is 0.59% (2.76 mm) with a standard deviation of 1.77% (8.09 mm). The Euclidean error is greater than the perimetric error due to error propagation when calculating the vertex positions from the side lengths. Tightly integrating the sensors eliminates the error from sensor attachment, so these skins exhibit high accuracy in proprioception.

We conducted the experiments to validate the skins' sensing separately from their actuation to avoid coupling effects. A limitation of this work is the skins' inability to reliably reconstruct shape during actuation because the strain sensors respond to the actuators' inflation as well as the stretching of the skin. Future work will involve modeling to optimize the sensor placement relative to the pneumatic bladders in order to mitigate the coupling effect, a strategy employed in [19].

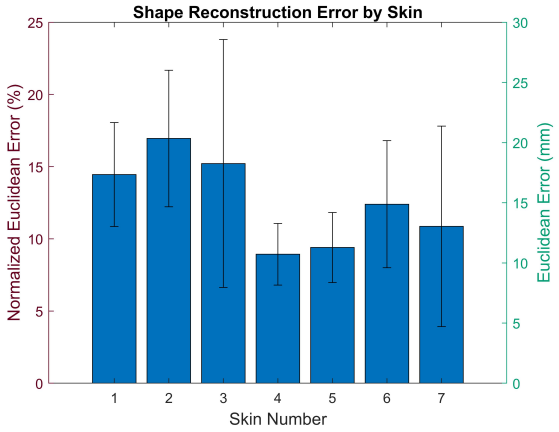

[a]

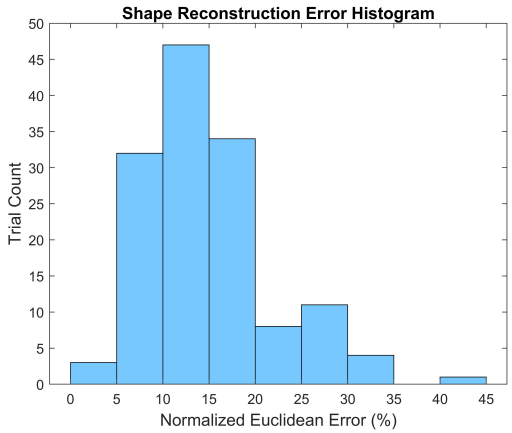

[b]

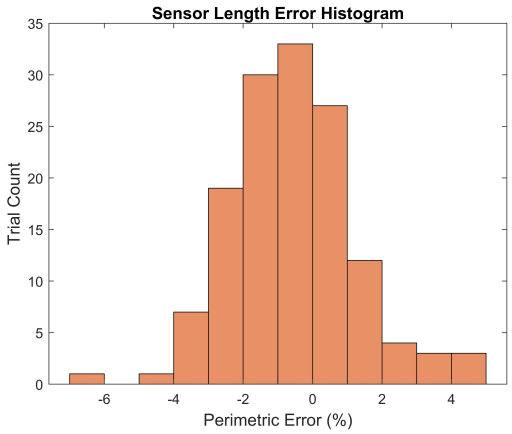

[c]

Fig. 4. Error analysis. [a] The Euclidean error is plotted for each skin. The left axis is normalized by the rest length (120 mm) of one side of the skin. [b] The normalized Euclidean error is plotted in a histogram for all trials across all skins. $\mu = 12.6\%$; $\sigma = 5.80\%$. [c] The perimetric error is plotted in a histogram for all trials across all skins. $\mu = 0.59\%$; $\sigma = 1.77\%$.

V. Conclusion

This work presents tightly integrated strain sensing in robotic skins. Experiments demonstrate high reliability in shape reconstruction due to the tight integration. This work is an important step toward fully integrated robotic skins with robust feedback control.

REFERENCES

[1] J. W. Booth, D. Shah, J. C. Case, E. L. White, M. C. Yuen, O. Cyr-Choiniere, and R. Kramer-Bottiglio, "Omniskins: Robotic skins that turn inanimate objects into multifunctional robots," *Science Robotics*, vol. 3, no. 22, 2018.

[2] J. W. Booth, O. Cyr-Choiniere, J. C. Case, D. Shah, M. C. Yuen, and R. Kramer-Bottiglio, "Surface actuation and sensing of a tensegrity structure using robotic skins," *Soft Robotics*, 2020.

[3] J. C. Case, J. Gibert, J. Booth, V. SunSpiral, and R. Kramer-Bottiglio, "Spinal helical actuation patterns for locomotion in soft robots," *IEEE Robotics and Automation Letters*, vol. 5, no. 3, pp. 3814–3821, 2020.

[4] D. S. Shah, M. C. Yuen, L. G. Tilton, E. J. Yang, and R. Kramer-Bottiglio, "Morphing robots using robotic skins that sculpt clay," *IEEE Robotics and Automation Letters*, vol. 4, no. 2, pp. 2204–2211, 2019.

[5] J. C. Case, M. C. Yuen, J. Jacobs, and R. Kramer-Bottiglio, "Robotic skins that learn to control passive structures," *IEEE Robotics and Automation Letters*, vol. 4, no. 3, pp. 2485–2492, 2019.

[6] B. Shih, D. Shah, J. Li, T. G. Thuruthel, Y.-L. Park, F. Iida, Z. Bao, R. Kramer-Bottiglio, and M. T. Tolley, "Electronic skins and machine learning for intelligent soft robots," *Science Robotics*, vol. 5, no. 41, 2020.

[7] E. L. White, J. C. Case, and R. K. Kramer, "Multi-element strain gauge modules for soft sensory skins," *IEEE Sensors Journal*, vol. 16, no. 8, pp. 2607–2616, 2015.

[8] B. Shih, D. Drotman, C. Christianson, Z. Huo, R. White, H. I. Christensen, and M. T. Tolley, "Custom soft robotic gripper sensor skins for haptic object visualization," in *2017 IEEE/RSJ international conference on intelligent robots and systems (IROS)*. IEEE, 2017, pp. 494–501.

[9] R. A. Bilodeau, E. L. White, and R. K. Kramer, "Monolithic fabrication of sensors and actuators in a soft robotic gripper," in *2015 IEEE/RSJ International Conference on Intelligent Robots and Systems (IROS)*. IEEE, 2015, pp. 2324–2329.

[10] D. Hughes and N. Correll, "A soft, amorphous skin that can sense and localize textures," in *2014 IEEE International Conference on Robotics and Automation (ICRA)*. IEEE, 2014, pp. 1844–1851.

[11] Y.-L. Park, B.-r. Chen, and R. J. Wood, "Soft artificial skin with multi-modal sensing capability using embedded liquid conductors," in *SENSORS, 2011 IEEE*. IEEE, 2011, pp. 81–84.

[12] Y.-L. Park, B.-R. Chen, and R. J. Wood, "Design and fabrication of soft artificial skin using embedded microchannels and liquid conductors," *IEEE Sensors journal*, vol. 12, no. 8, pp. 2711–2718, 2012.

[13] M. A. McEvoy and N. Correll, "Materials that couple sensing, actuation, computation, and communication," *Science*, vol. 347, no. 6228, 2015.

[14] S. Y. Kim, R. Baines, J. Booth, N. Vasios, K. Bertoldi, and R. Kramer-Bottiglio, "Reconfigurable soft body trajectories using unidirectionally stretchable composite laminae," *Nature communications*, vol. 10, no. 1, pp. 1–8, 2019.

[15] H. Wang, M. Totaro, and L. Beccai, "Toward perceptive soft robots: Progress and challenges," *Advanced Science*, vol. 5, no. 9, p. 1800541, 2018.

[16] J. Shintake, E. Piskarev, S. H. Jeong, and D. Floreano, "Ultrastretchable strain sensors using carbon black-filled elastomer composites and comparison of capacitive versus resistive sensors," *Advanced Materials Technologies*, vol. 3, no. 3, p. 1700284, 2018.

[17] A. Tairych and I. A. Anderson, "Capacitive stretch sensing for robotic skins," *Soft robotics*, vol. 6, no. 3, pp. 389–398, 2019.

[18] R. A. Bilodeau, A. M. Nasab, D. S. Shah, and R. Kramer-Bottiglio, "Uniform conductivity in stretchable silicones via multiphase inclusions," *Soft matter*, vol. 16, no. 25, pp. 5827–5839, 2020.

[19] R. A. Bilodeau, M. C. Yuen, J. C. Case, T. L. Buckner, and R. Kramer-Bottiglio, "Design for control of a soft bidirectional bending actuator," in *2018 IEEE/RSJ International Conference on Intelligent Robots and Systems (IROS)*. IEEE, 2018, pp. 1–8.